Electronic Supplementary Material (ESI) for Materials Advances.

Electronic Supplementary Information

Zinc-triggered photocatalytic selective synthesis of benzyl acetate on inverse spinel $CuFe_2O_4$ 3D networks: a case of coupled redox photocatalytic reaction

Yihan Zhang[a, †], Jingqi Tian[a, †], Tengfei Jiang*[a], Huaiguo Xue[a]

School of Chemistry and Chemical Engineering, Yangzhou University, 180 Siwangting Road, Yangzhou 225002, People's Republic of China. Email: jiangtengfei@yzu.edu.cn

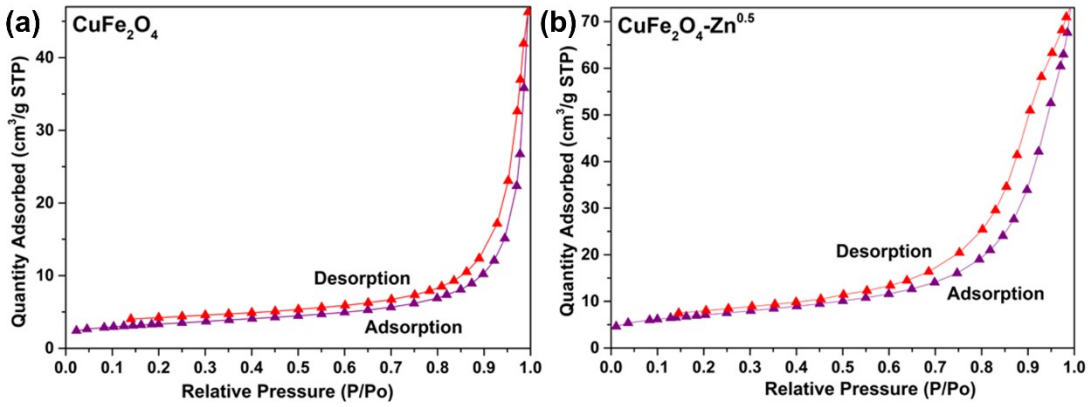

Fig.S1. N_2 adsorption-desorption isotherms of $CuFe_2O_4$ (a) and $CuFe_2O_4$-$Zn^{0.5}$ (b).

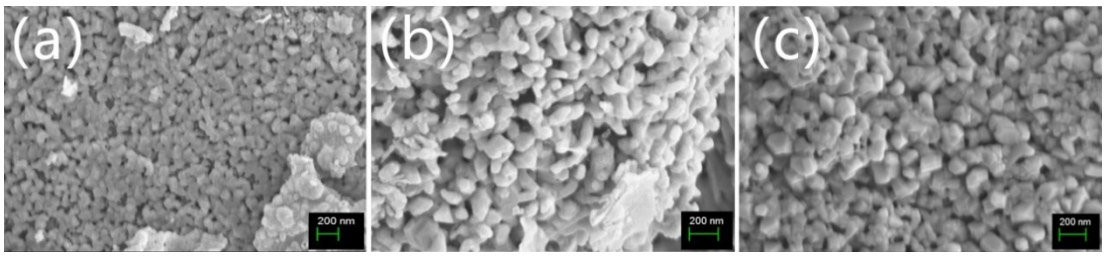

Fig. S2. The SEM of samples $CuFe_2O_4$-$Zn^{0.3}$ (a), $CuFe_2O_4$-$Zn^{1.0}$ (b), $CuFe_2O_4$-$Zn^{1.5}$ (c).

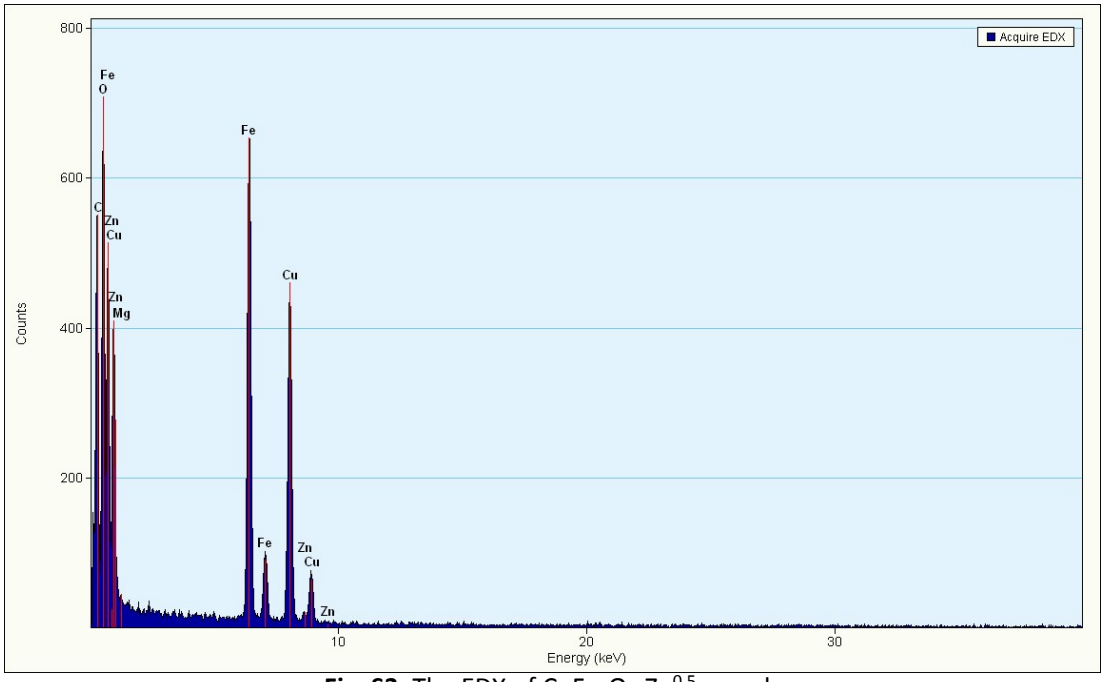

Fig. S3. The EDX of $CuFe_2O_4$-$Zn^{0.5}$ sample.

Table S1. Elemental analysis of samples $CuFe_2O_4$-$Zn^{0.5}$.

Element	Weight %	Atomic %	Uncert. %	Detector Correction	k-Factor
O(K)	30.81	62.22	0.44	0.49	2.008
Fe(K)	37.27	21.56	0.36	0.99	1.359
Cu(K)	30.92	15.72	0.36	0.99	1.601
Zn(K)	0.98	0.48	0.08	0.99	1.686

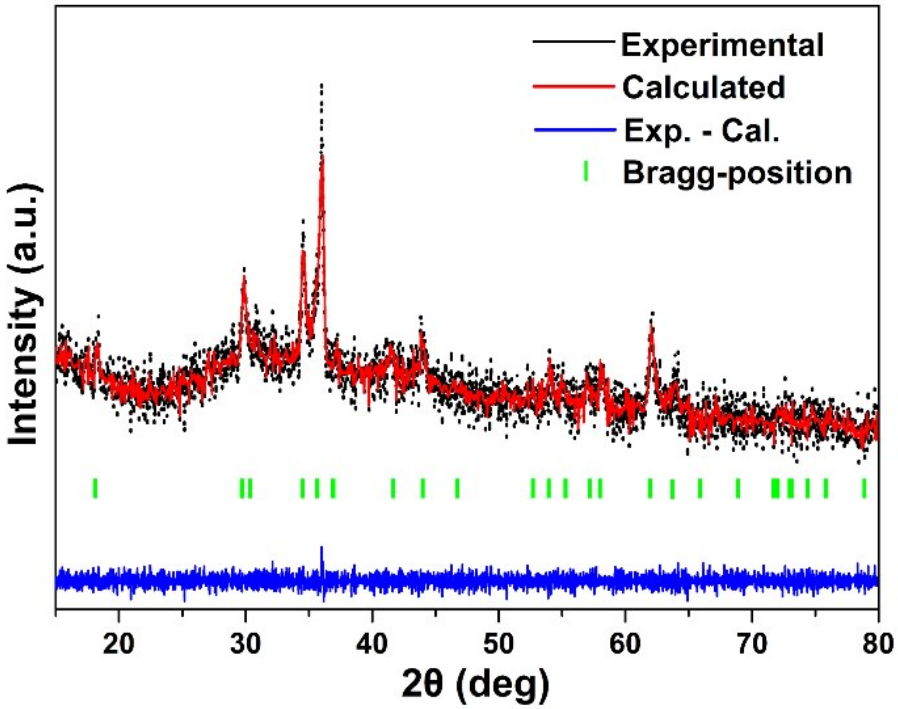

Fig. S4. Rietveld refinement of XRD pattern of $CuFe_2O_4$ sample.

Table S2. Rietveld refinement results of pure $CuFe_2O_4$.

Sample	Refinement data				Lattice parameters		Density
	sig	R_b	R_{wp}	R_{exp}	a	c	
$CuFe_2O_4$	1.04	4.53	5.68	4.96	5.94687	8.42621	5.383

Table S3. The ratio of $Fe^{II}/(Fe^{II} + Fe^{III})$ and oxygen vacancy/total oxygen from XPS fitting.

Entry	$Fe^{II}/(Fe^{II} + Fe^{III})$ (%)	Oxygen vacancy/Total oxygen (%)
$CuFe_2O_4$	49.42	18.34
$CuFe_2O_4$-$Zn^{0.3}$	58.75	20.70
$CuFe_2O_4$-$Zn^{0.5}$	71.76	35.47
$CuFe_2O_4$-$Zn^{1.0}$	65.58	32.31
$CuFe_2O_4$-$Zn^{1.5}$	44.49	16.48

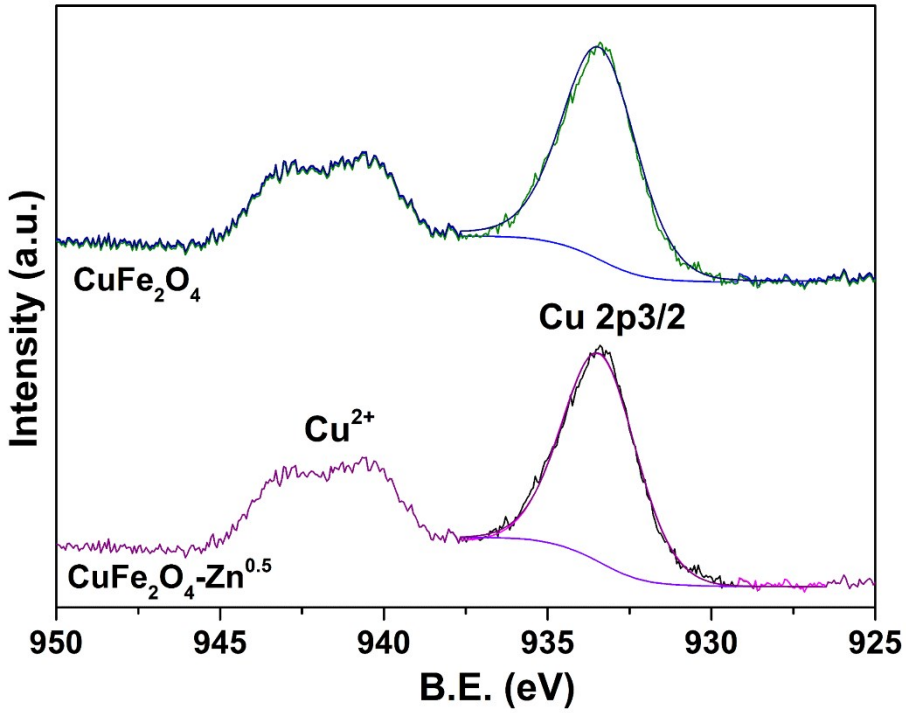

Fig. S5. High resolution XPS spectra of Cu 2p spectra in pure $CuFe_2O_4$ and $CuFe_2O_4$-$Zn^{0.5}$.

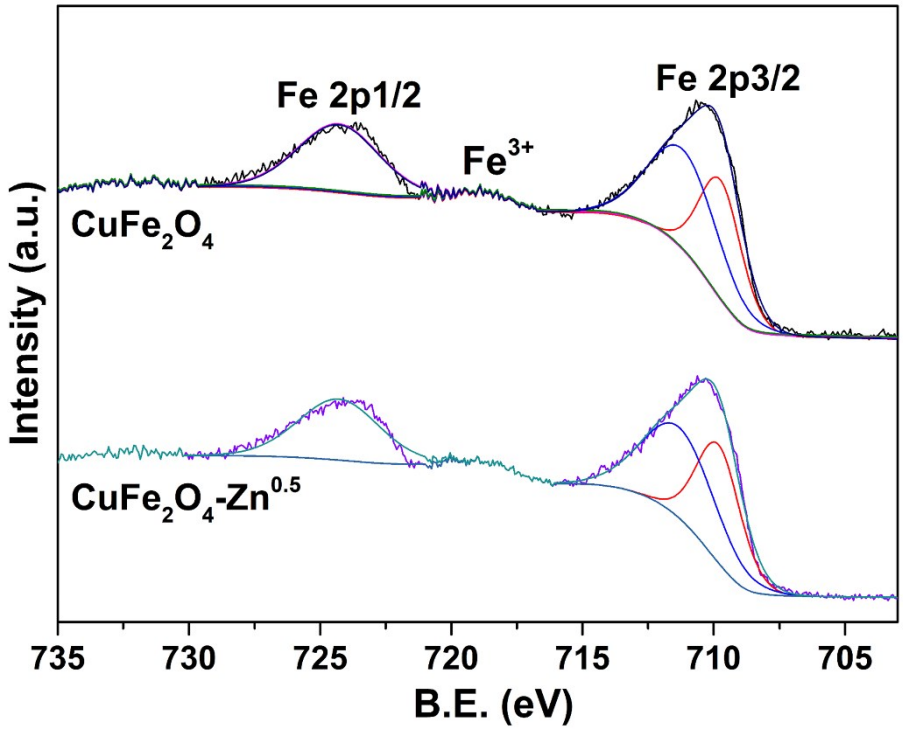

Fig.S6. High resolution XPS spectra of Fe 2p spectra in pure $CuFe_2O_4$ and $CuFe_2O_4$-$Zn^{0.5}$.

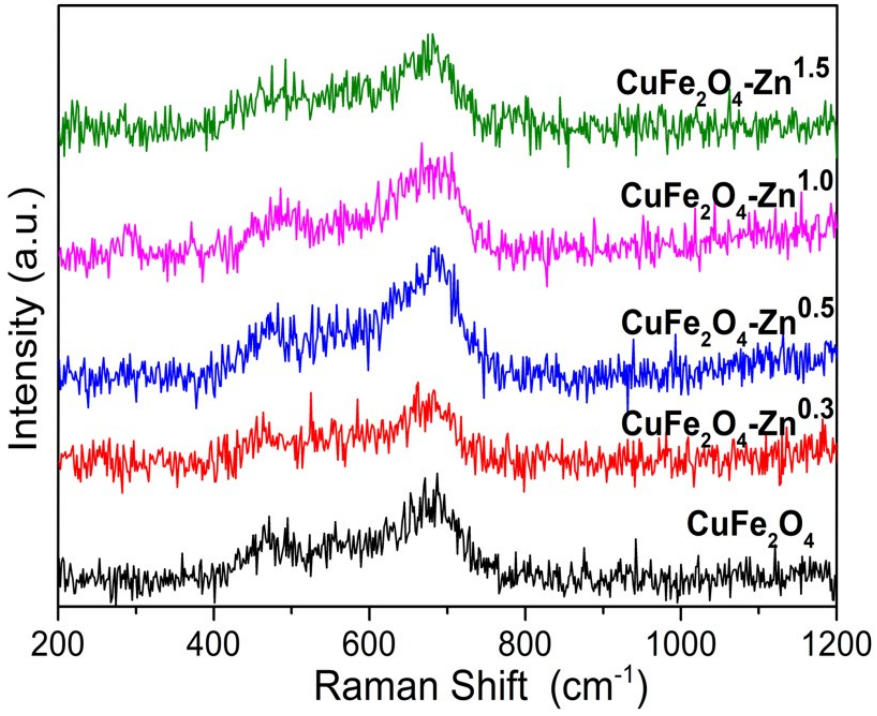

Fig. S7. The Raman spectra of $CuFe_2O_4$, $CuFe_2O_4$-$Zn^{0.3}$, $CuFe_2O_4$-$Zn^{0.5}$, $CuFe_2O_4$-$Zn^{1.0}$ and $CuFe_2O_4$-$Zn^{1.5}$.

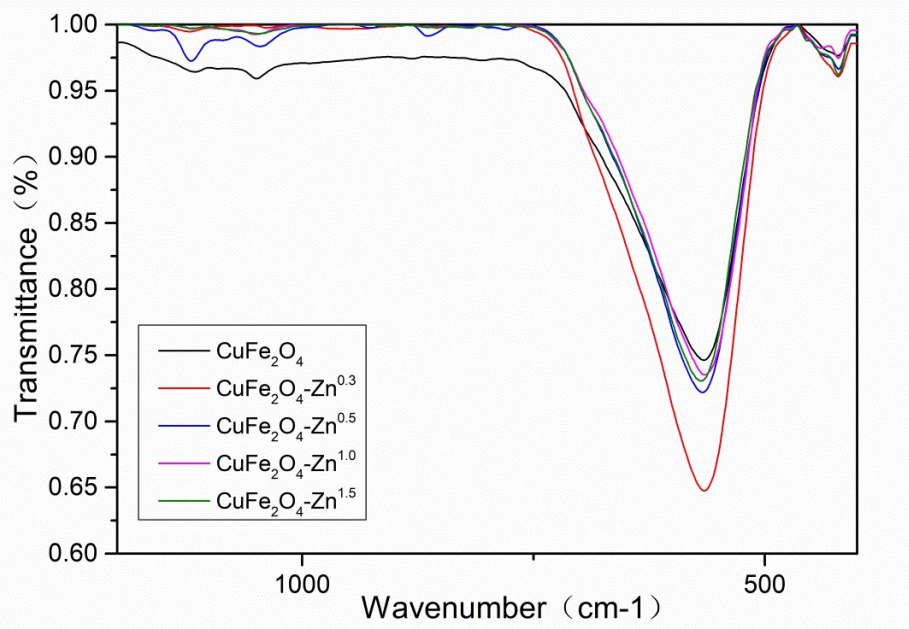

Fig. S8. Infrared spectra of $CuFe_2O_4$, $CuFe_2O_4$-$Zn^{0.3}$, $CuFe_2O_4$-$Zn^{0.5}$, $CuFe_2O_4$-$Zn^{1.0}$ and $CuFe_2O_4$-$Zn^{1.5}$.

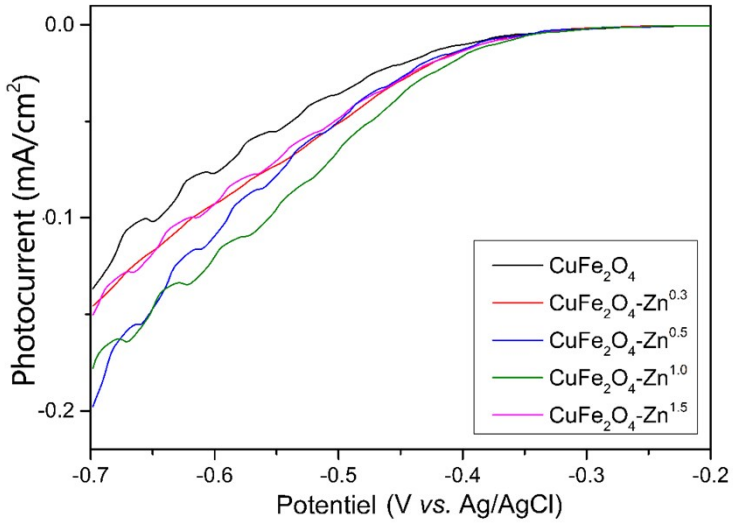

Fig. S9. LSV curves of $CuFe_2O_4$, $CuFe_2O_4$-$Zn^{0.3}$, $CuFe_2O_4$-$Zn^{0.5}$, $CuFe_2O_4$-$Zn^{1.0}$ and $CuFe_2O_4$-$Zn^{1.5}$.

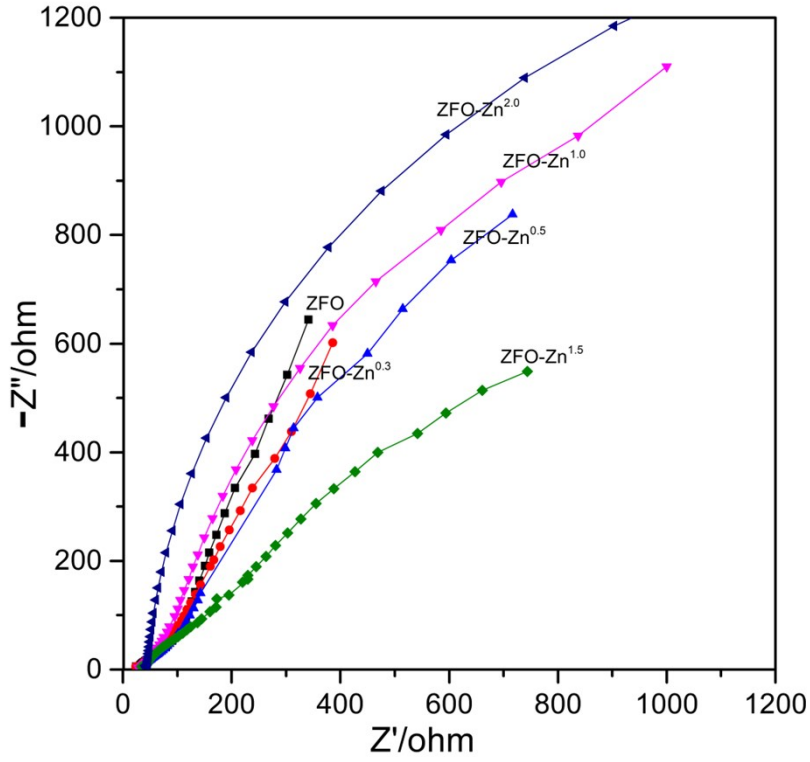

Fig. S10. The Z'--Z" plots of $CuFe_2O_4$, $CuFe_2O_4$-$Zn^{0.3}$, $CuFe_2O_4$-$Zn^{0.5}$, $CuFe_2O_4$-$Zn^{1.0}$ and $CuFe_2O_4$-$Zn^{1.5}$.

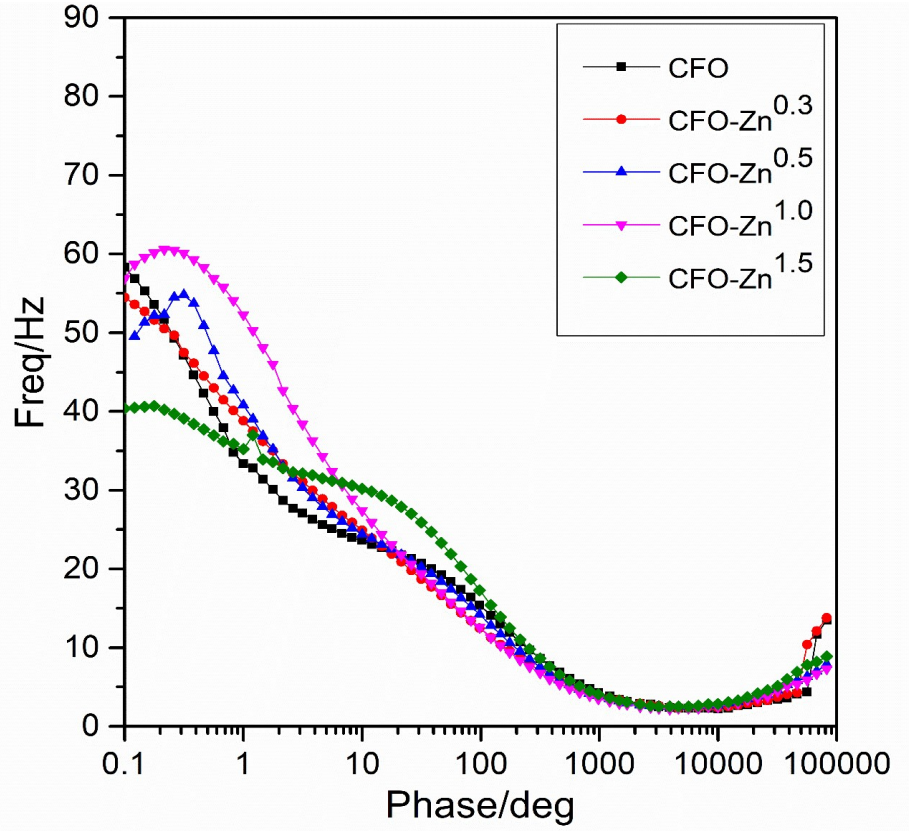

Fig. S11. The Phase-Freq of $CuFe_2O_4$, $CuFe_2O_4$-$Zn^{0.3}$, $CuFe_2O_4$-$Zn^{0.5}$, $CuFe_2O_4$-$Zn^{1.0}$ and $CuFe_2O_4$-$Zn^{1.5}$.

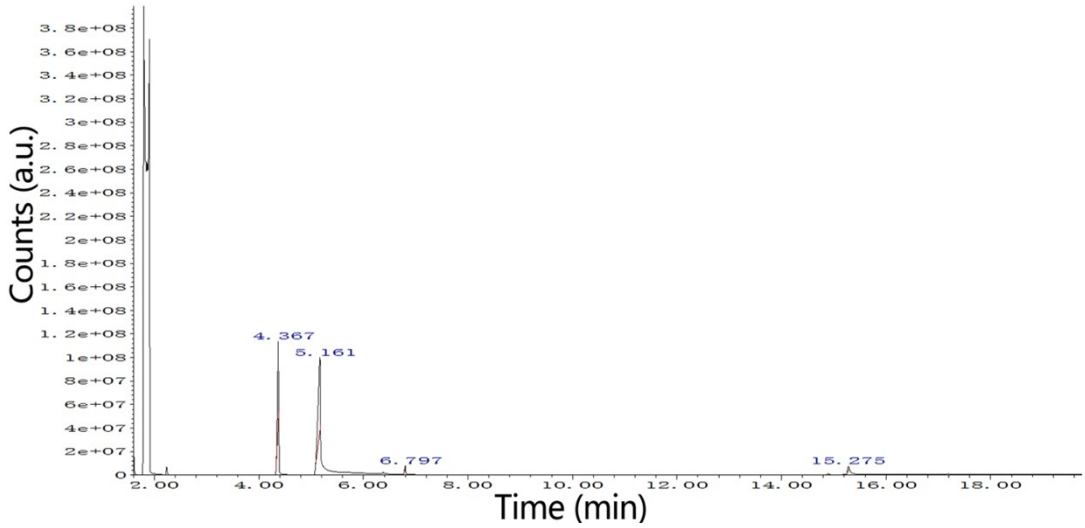

Fig. S12. GC-MS spectrum of samples $CuFe_2O_4$

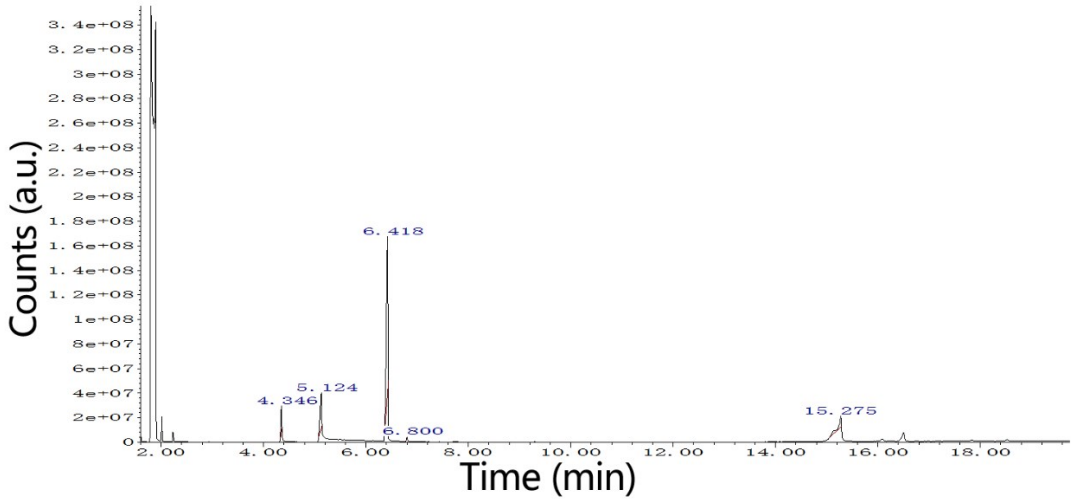

Fig. S13. GC-MS spectrum of samples $CuFe_2O_4$-$Zn^{0.5}$.

Table S4. Analysis of GC-MS spectrum results of samples $CuFe_2O_4$.

Compound number	Retention time (min)	Scan number	Area (AB * s)	Baseline height (AB)	Absolute height (AB)	Peak width 50% (min)	Start time (min)	End time (min)	Peak type
1	4.368	256	884628589	72312175	114583606	0.02	4.325	4.379	M
2	5.161	329	1762227644	64916149	100268784	0.045	5.08	5.179	M
3	6.801	480	19093565	3624088	8368978	0.009	6.78	6.805	M
4	15.275	1260	55026384	4383054	7886679	0.021	15.253	15.296	M

Table S5. Analysis of GC-MS spectrum results of samples $CuFe_2O_4$-$Zn^{0.5}$

Compound number	Retention time (min)	Scan number	Area (AB * s)	Baseline height (AB)	Absolute height (AB)	Peak width 50% (min)	Start time (min)	End time (min)	Peak type
1	4.346	254	175357377	21422287	29659414	0.014	4.325	4.359	M
2	5.128	326	541241349	31768248	42836648	0.028	5.076	5.138	M
3	6.421	445	2551266298	132680022	170465277	0.032	6.364	6.437	M
4	6.801	480	12187494	2151176	4519380	0.009	6.782	6.808	M
5	15.275	1260	306101651	9133878	21352626	0.056	15.06	15.29	M

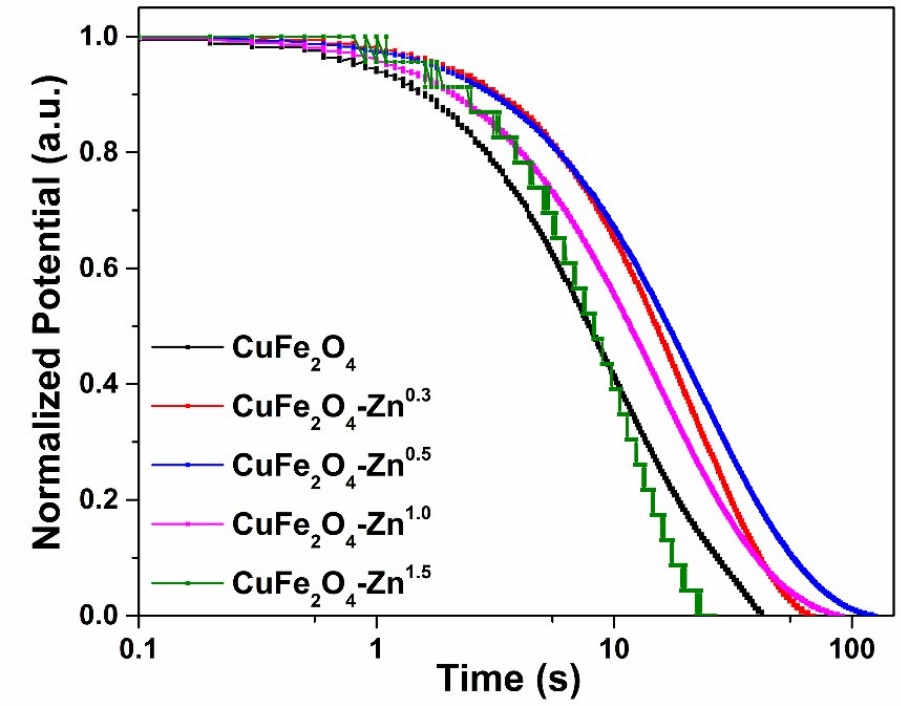

Fig. S14. Open circuit potential decay curves of $CuFe_2O_4$, $CuFe_2O_4$-$Zn^{0.3}$, $CuFe_2O_4$-$Zn^{0.5}$, $CuFe_2O_4$-$Zn^{1.0}$ and $CuFe_2O_4$-$Zn^{1.5}$.

Table S6. The lifetime (τ) of the photoexcited electrons of $CuFe_2O_4$, $CuFe_2O_4$-$Zn^{0.3}$, $CuFe_2O_4$-$Zn^{0.5}$, $CuFe_2O_4$-$Zn^{1.0}$ and $CuFe_2O_4$-$Zn^{1.5}$.

Sample	τ (s)
$CuFe_2O_4$	11.39
$CuFe_2O_4$-$Zn^{0.3}$	21.67
$CuFe_2O_4$-$Zn^{0.5}$	24.42
$CuFe_2O_4$-$Zn^{1.0}$	16.84
$CuFe_2O_4$-$Zn^{1.5}$	13.18

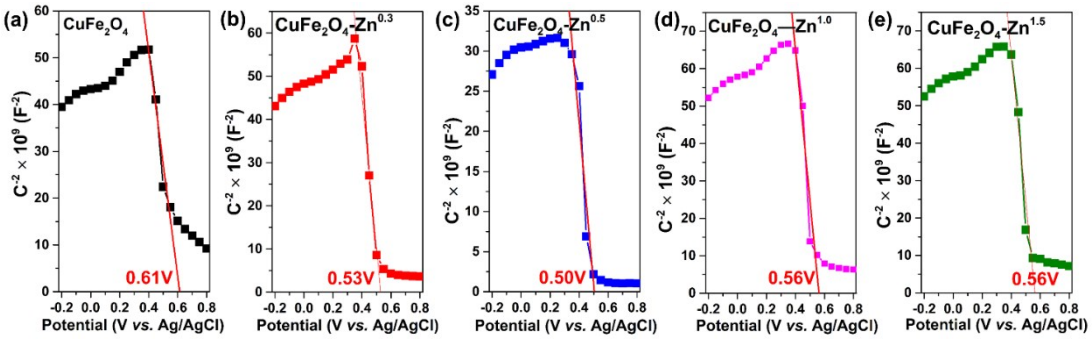

Fig. S15. Mott-Schottky plots of $CuFe_2O_4$ (a), $CuFe_2O_4$-$Zn^{0.3}$ (b), $CuFe_2O_4$-$Zn^{0.5}$ (c), $CuFe_2O_4$-$Zn^{1.0}$ (d) and $CuFe_2O_4$-$Zn^{1.5}$ (e).

Table S7. Control experiments of selective synthesis of benzyl acetate by using $CuFe_2O_4$-$Zn^{0.5}$ sample.

Entry	Reactants	Scavenger	Light	Product	Selectivity (%)
1	Benzaldehyde + Acetic acid	Methanol	White	Benzyl acetate	70.55
2	Benzaldehyde + Acetone	Methanol	White	Benzyl acetate	0.24
3	Benzaldehyde + Isopropanol	-	Without	Benzyl acetate	0

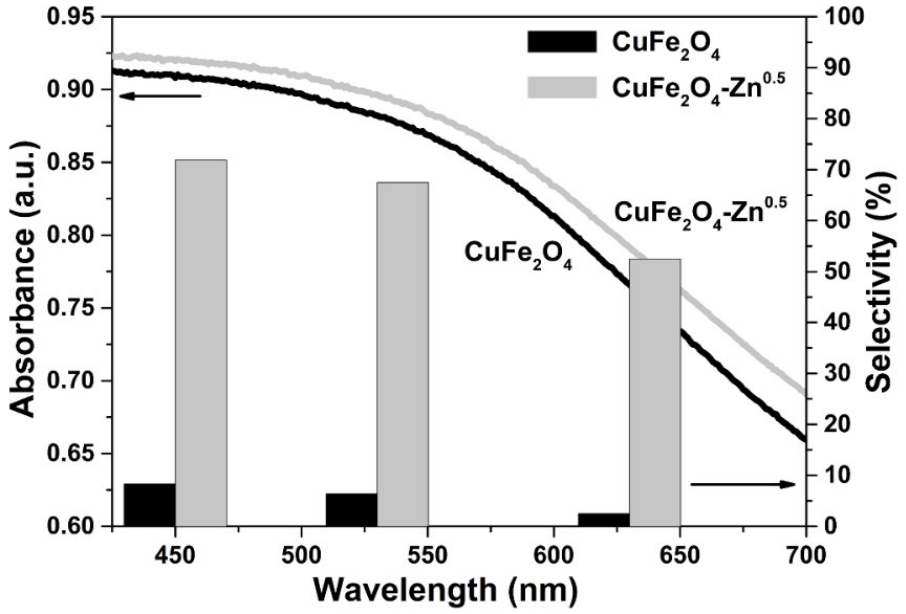

Fig. S16. The photocatalytic selectivity for benzyl acetate synthesis as a function of the wavelength of the incident light.

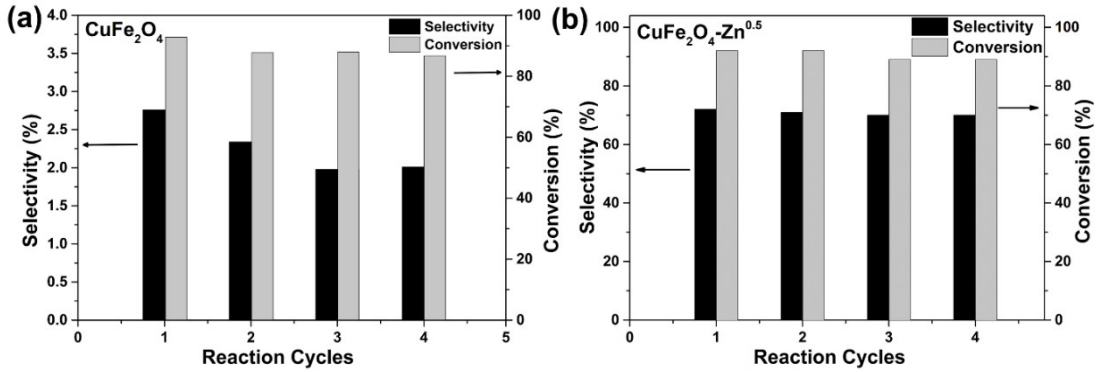

Fig. S17. Recyclability of (a) $CuFe_2O_4$ and (b) $CuFe_2O_4$-$Zn^{0.5}$ sample in photocatalytic selective synthesis of benzyl acetate.

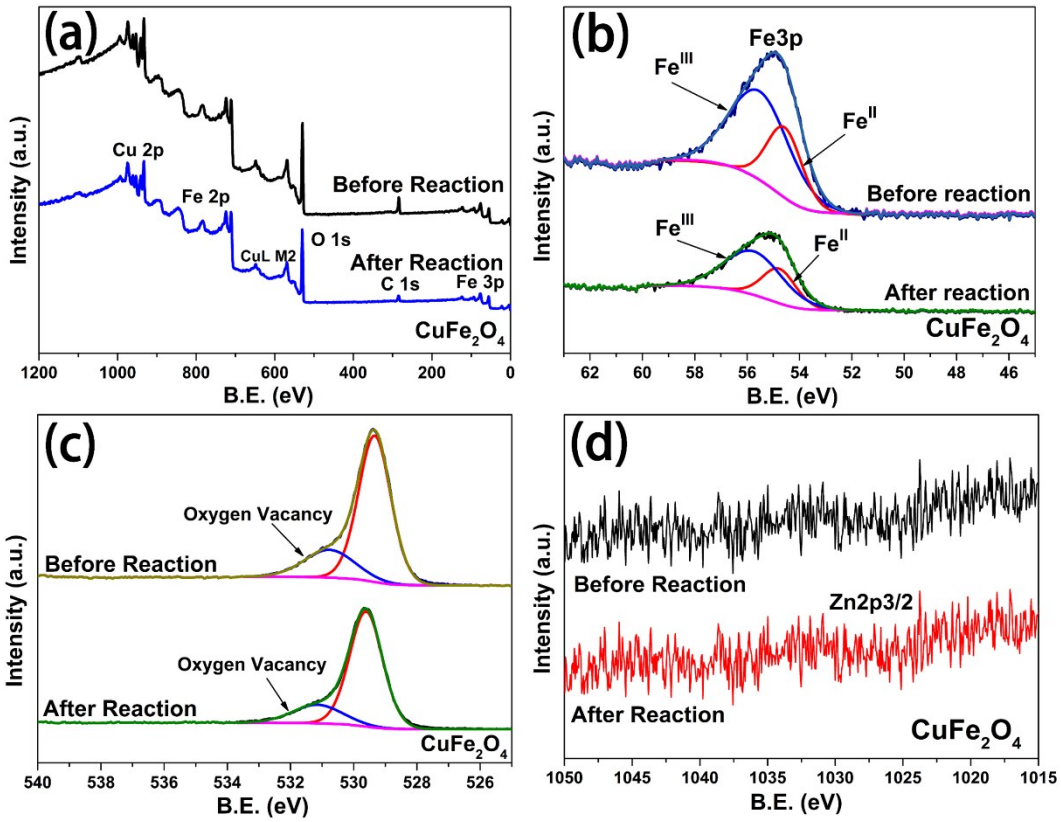

Fig. S18. XPS survey (a), Fe 3p (b), O 1s (c), and Zn 2p (d) spectra of pure $CuFe_2O_4$ before and after recycling test.

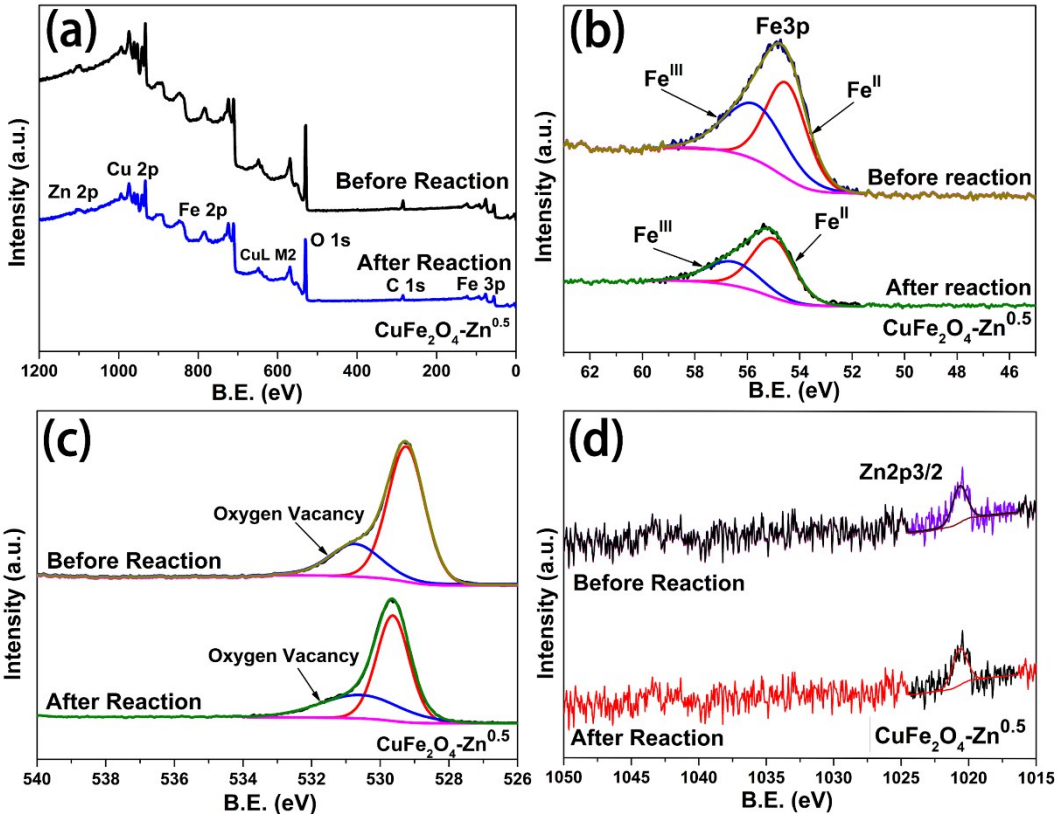

Fig. S19. XPS survey (a), Fe 3p (b), O 1s (c), and Zn 2p (d) spectra of $CuFe_2O_4$-$Zn^{0.5}$ before and after recycling test.

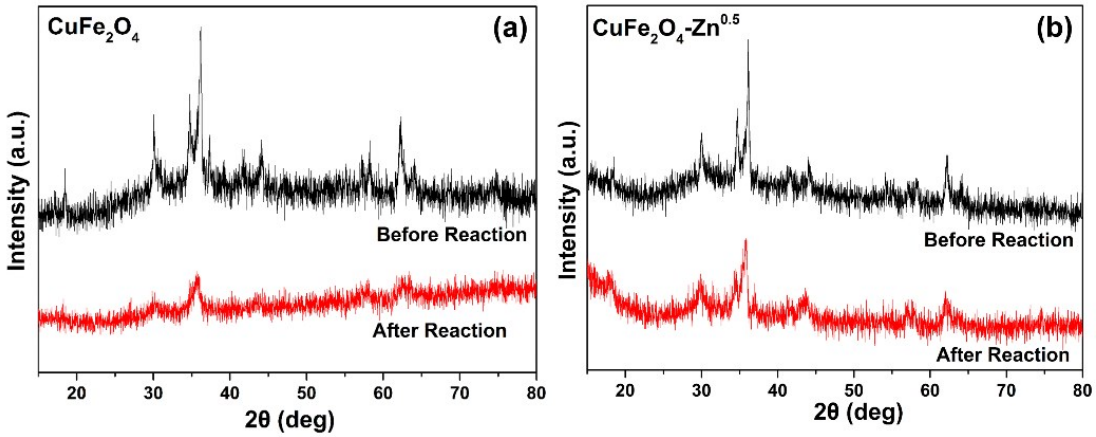

Fig. S20. XRD patterns of $CuFe_2O_4$ (a) and $CuFe_2O_4$-$Zn^{0.5}$ (b) before and after recycling test.